Northern Michigan University
The Commons

Journal Articles

3-2011

A stand-alone Method for Anatomical Localization of NIRS Measurements

Tomer Fekete

Denis Rubin

Joshua M. Carlson
joshcarl@nmu.edu

Lilianne R. Mujica-Parodi

Follow this and additional works at: http://commons.nmu.edu/facwork_journalarticles

Recommended Citation

A stand-alone method for anatomical localization of NIRS measurements

4 authors:

Tomer Fekete
University of Leuven
16 PUBLICATIONS   135 CITATIONS

SEE PROFILE

Denis Rubin
New York University
24 PUBLICATIONS   304 CITATIONS

SEE PROFILE

Joshua M Carlson
Northern Michigan University
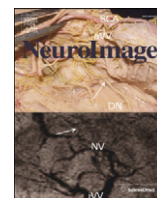49 PUBLICATIONS   706 CITATIONS

SEE PROFILE

Lilianne R Mujica-Parodi
Stony Brook University
84 PUBLICATIONS   1,119 CITATIONS

SEE PROFILE

A stand-alone method for anatomical localization of NIRS measurements

Tomer Fekete [a], Denis Rubin [b], Joshua M. Carlson [a], Lilianne R. Mujica-Parodi [a,*]

[a] Department of Biomedical Engineering, State University of New York at Stony Brook, Stony Brook, NY 11794-5291, USA
[b] Department of Applied Mathematics and Statistics, State University of New York at Stony Brook, Stony Brook, NY 11794–3690, USA

ARTICLE INFO

ABSTRACT

Near-infrared spectroscopy (NIRS) is a non-invasive cortical imaging technique that provides many of the advantages of cortical fMRI with additional benefits of low cost, portability, and increased temporal resolution—features that make it potentially ideal for clinical diagnostic applications. However, the usefulness of NIRS is contingent on the ability to reliably localize the measured signal cortically. Although this can be achieved by supplementing NIRS data collection with an MRI scan, a much more appealing alternative is to use a portable magnetic measuring system to record the locations of optodes. Previous work has shown that optode skull measurements can be projected to the brain consistently within reasonable error bounds. Yet, as we show, if this is done without explicitly modeling the geometry of the holder securing the NIR optodes to participants' heads, considerable bias in the projection loci results. Here, we describe an algorithm that not only overcomes this bias but also corrects for measurement error in both optode position and skull reference points (which are used to register the measurements to standard brain templates) by applying geometric constraints. This method has been implemented as part of our NIRS Analysis Package (NAP), a public domain Matlab toolbox for analysis of NIRS data.

© 2011 Published by Elsevier Inc.

Introduction

Near-infrared spectroscopy (for a recent review, see Huppert et al., 2009; NIRS, Jobsis, 1977) is a non-invasive cortical imaging technique that measures brain oxygenated and deoxygenated hemoglobin concentrations. In the wake of an ever-increasing volume of functional magnetic resonance imaging (fMRI) studies within neuroscience research, recent years have also seen a marked increase in the use of NIRS in human imaging studies. Although similar to fMRI in that it measures aspects of the hemodynamic response, NIRS offers several notable advantages: (1) portability for utilization in more ecological settings with less compliant participants (for example, young children), (2) superior temporal resolution, and (3) lower purchase and operating costs as compared to fMRI. These improvements come at a price—not only does NIRS suffer from limited spatial resolution (Cope et al., 1988; Fukui et al., 2003; Okada and Delpy, 2003a, b), but in itself does not enable exact localization of the measured activity within the cortex. One solution to this problem is co-registering NIRS measurements with fMRI scans, but the necessity to do so thereby defeats many of NIRS's important strengths.

One of the most promising alternatives that circumvents this problem is the use of a 3D magnetic space digitizer to obtain relative locations of 10–20 standard markers (Jasper, 1958) and the NIR optodes in a real-world coordinate system. In principle, this information should suffice to register the measurements to canonical brain templates, such as the Montreal Neurological Institute (MNI) template. Yet measurements provide the location of the optode tips on the skull, rather than the loci from which the signal originates within the brain. Thus, it is necessary to project the optode contact points onto the cortical surface before the origin of the NIRS signals can be established. In a series of elegant studies, Okamoto, Singh and colleagues showed that optode loci can be projected consistently to MNI space (Okamoto et al., 2004; Okamoto and Dan, 2005; Singh et al., 2005). Using a database of 17 reference brains, they established the error bounds of their projection method (the balloon inflation method) to be within reasonable limits (~1 cm).

However, as we show below, the use of approximate methods of projection, rather than explicitly computing surface normals to guide projection, can result in considerable bias. Moreover, projection inaccuracies can be aggravated by additional factors, mainly measurement errors occurring in the process of recording the positions of the optodes and the 10–20 system markers on the skull.

First, error in localizing the 10–20 markers will result in a flawed estimate of the structure of the participants' skulls and brains. This is because both of these structures are estimated solely on the basis of the 10–20 markers. For example, error in the position of the markers can result in warping of the estimated brain shape (contraction, stretching, skewness, etc.). One of the clear marks of such errors is

* Corresponding author. Laboratory for the Study of Emotion and Cognition, Dept. of Biomedical Engineering, State University of New York at Stony Brook, School of Medicine, Bioengineering Building, Stony Brook, NY 11794-5281, USA. Tel.: +1 631 632 8577; fax: +1 444 6646.
E-mail address: lmujicaparodi@gmail.com (L.R. Mujica-Parodi).

exaggerated distance between the optode loci and the estimated skull surface. As a result, for optode loci to be projected to the cortical surface they must first be projected to the skull surface. Yet, a single measurement does not, by itself, afford the information to do so reliably. In NIRS experiments, optodes are held in place against participants' heads by an optode holder. Therefore, one way to alleviate this difficulty is to utilize all of the measured optode loci to reconstruct the surface of the optode holder. This would enable the computation of normals to this surface, which in turn would enable the projection of optodes: first to the skull, and from there to the cortical surface. Unfortunately, measurement errors in the positions of the optodes will compromise not only the localization accuracy of each optode position itself but, worse still, will result in over- or under-estimation of the curvature of the holder at the projection loci, which in turn will lead to in inaccuracy in the estimate of the radiation angle. Therefore it would seem that not only does accurate localization of measurements necessitate explicit reconstruction of the optode holder structure but, to do so reliably, it is necessary to overcome the errors consequent to measuring both optode positions and the position of the 10–20 markers.

A hint as to how this may be done is found in the structure of the optode holders: optode holders are constructed from flexible materials to accommodate differing skull shapes and shafts are normally evenly spaced on parallel geodesic curves along the surface of the holder (akin to longitude and latitude line intersections on a globe). Such well-defined geometric features in the optode positions can be used to reduce the measurement errors associated with determining the position of each optode shaft.

In what follows we describe an algorithm that targets the explicit modeling of the optode holder. Hence, it combines not only an unbiased projection method but also incorporates several denoising procedures that enable one to increase the accuracy of cortical localization. The proposed method results from forcing the initial measurements to conform to the following ground truths: (1) optode loci should conform to the actual configuration of optode shafts within the holder, (2) optodes actually make contact with the skull at the time of measurement, and (3) optodes are perpendicular to the holder surface and therefore directly reflect the geometry of the optode model (which as a result of 1 and 2 is a smooth approximation of the skull shape). This algorithm is incorporated in our NIRS Analysis Package (NAP), a publicly available MATLAB-based toolbox for analysis of near-infrared spectroscopy data (http://lsec.neuropraxia.webfactional.com/Software_and_Instrumentation.html).

Methods

Experimental materials and methods

Participants

We recruited 12 adults (three females), ages 23–39 to participate in the experiment. All subjects were healthy and free of neurological or cardiovascular illness. This study was approved by the institutional review board of Stony Brook University; all participants provided informed consent.

Data acquisition

An ETG 4000 (Hitachi, Tokyo) 33 optode holder was placed occipitally and secured using a custom-made cap. To reduce movement, participants' heads were stabilized using a custom-made head-holder. Optode locations were measured using a Polhemus ISOTRAK II (Inition, London) magnetic tracker, controlled by thean ETG 4000 in the 33 detectors (52 channels) configuration. The 10–20 markers (Jasper, 1958) measured were Nz (*nasion*), Iz (*inion*), AR (*right ear*), AL (*left ear*), and Cz (*midpoint of the crown of the head*).

MNI template

The skull and cortical surface sets of points in MNI space from Okamoto et al. (2004) were used for all reported computations.

Reference brain data base

The structural data in Okamoto et al. (2004) from 17 brains were used to determine the error bounds of optode positions.

Data analysis

Data analyses were carried out using Matlab R2010a (Mathworks, Natick, MA).

Approximate projection methods

Nearest neighbor projection

The nearest neighbor method is simply finding the nearest point on the cortical surface to each optode locus.

Cortical expansion

The cortical expansion method is finding the point on the cortex that when multiplied with a scalar is closest to the optode position:

$$proj(opt) = \arg\min_{v \in ctx} \left(\arg\min_{a} d(opt, av) \right) = \arg\min_{v \in ctx} \left(\frac{opt \cdot v}{v \cdot v} \right)$$

where *opt* denotes the optode position and *ctx* denotes the cortical surface after subtraction of its centroid.

It is important to note that in the case of two concentric spheres these methods coincide with projection along the normal.

The balloon inflation method

This algorithm, as described by Okamoto and Singh et al. (Okamoto et al., 2004, 2005; Singh et al., 2005), defines the range of the cortical surface region by selecting certain numbers of cortical surface points that are closest from a given head-surface point (P). Conceptually, if one drew a sphere from a given head-surface point and inflated it gradually like a balloon, it would cover a certain portion of the cortical surface in a similar manner. Two hundred cortical surface points closest to a given head-surface point (P) that roughly cover the cortical region with a radius of 1 cm are selected. Next the coordinate values for the points are averaged to yield their centroid (P_{ce}). A virtual rod ($r = 1$ mm) through the P_{ce} and P is taken, and the intersection with the cortical surface found. P_c was identified as the average of the coordinate values of the three points closest to P, chosen from among the cortical surface points that were covered by the rod. Search is limited to within a range of 1000 points closest to P to prevent the inclusion of points representing an excessively deep cortical area or points arising from internal debris.

Forward and backward transformation into MNI space

If optodes are to be localized in MNI space, then the measured 10–20 reference points can be mapped to the corresponding loci in the MNI template by a least squares minimizing linear map (i.e., an affine transformation; cf. Okamoto et al., 2004). Let $\{r_1\ r_1\ \ldots\ r_k\}$ be a set of k anatomical reference points (e.g., In, Nz, …) in real-world coordinates and $\{R_1\ R_1\ \ldots\ R_k\}$ the corresponding points in MNI space. The regression problem writes as $X = \begin{bmatrix} x_{r1} & x_{r2} & \cdots & x_{rk} \\ y_{r1} & y_{r2} & \cdots & y_{rk} \\ z_{r1} & z_{r2} & \cdots & z_{rk} \\ 1 & 1 & \cdots & 1 \end{bmatrix}$ $Y = \begin{bmatrix} x_{R1} & x_{R2} & \cdots & x_{Rk} \\ y_{R1} & y_{R2} & \cdots & y_{Rk} \\ z_{R1} & z_{R2} & \cdots & z_{Rk} \\ 1 & 1 & \cdots & 1 \end{bmatrix}$ where the least squares solution is given by $B = YX^t (XX^t)^{-t}$. Accordingly, the estimates of the 10–20 reference points in MNI space are $\hat{Y} = \begin{bmatrix} \hat{x}_{R1} & \hat{x}_{R2} & \cdots & \hat{x}_{Rk} \\ \hat{y}_{R1} & \hat{y}_{R2} & \cdots & \hat{y}_{Rk} \\ \hat{z}_{R1} & \hat{z}_{R2} & \cdots & \hat{z}_{Rk} \\ 1 & 1 & \cdots & 1 \end{bmatrix} = BX.$

Yet, by the same token, the map B is uniquely associated with an inverse map (B^{-1}). The inverse transform can be used to estimate the participants' brain and skull surface in real-world coordinates. Let ctx_{MNI} and H_{MNI} denote the cortical and skull surface in MNI space. Therefore, the estimate of the participants' brain surface and skull surface will be given by $B^{-1}(ctx_{MNI})$ and $B^{-1}(H_{MNI})$, respectively.

Overview of the proposed method

The method we propose comprises several distinct phases: (1) correction of errors in optode locations, (2) correction of error in anatomical marker position, (3) fitting the optodes with an explicit model of the optode holder, (4) projection of this model to the cortical surface, and (5) computing the location of channels.

Correction of errors in optode locations

In our data we applied the following constraints: forcing optode rows to be parallel, forcing optodes to be evenly spaced on each row, and forcing each optode column to lie on a plane.

To force optode rows to be parallel, they are regressed to a least squares plane. Given a set of points $\{v_i\} = \{(x_i, y_i, z_i)\} \in \Re^3$ the least squares plane is given by the first two principal components of the data. Accordingly, projecting out the normal to this plane (i.e., the principle component associated with the smallest eigenvalue) forces a set of points to lie on the least squares plane. That is, if we denote the normal as $n = \underset{\|u\|=1}{\arg\min}\left\{\lambda | \hat{V}\hat{V}^t u = \lambda u\right\}$, where $\hat{V} = \begin{bmatrix} x_1 - \bar{x} \cdots x_k - \bar{x} \\ y_1 - \bar{y} \cdots y_k - \bar{y} \\ z_1 - \bar{z} \cdots z_k - \bar{z} \end{bmatrix}$, then the aligned set of measurements is given by $\hat{V} = V - n(n^t V)$. Therefore, to align all of the optode rows, the mean of each row must first be removed from the points it comprises and then the normal of the entire set of points is projected out. Finally, the original mean of each row is added to each row in turn.

Next, optode loci are spaced evenly along the spline curves connecting each row. This is done by fitting each optode row with a natural spline (see Appendix), parameterized to the interval [0 1]. Thus, the arc-length formula can be used to solve for k evenly spaced points $l(t_i) = \int_0^{t_i} \|\gamma'(t)\| dt \Big/ \int_0^1 \|\gamma'(t)\| dt = \frac{i-1}{k-1}$, where $\gamma'(t)$ is the tangent to the spline.

Finally, to force optode columns to lie on a plane they are first projected to the row plane. This is done by subtracting the mean from each optode row and then projecting each point on the first two principle components of the data (computed as described above). Next, each column (which in the new coordinates is 2D) is regressed to a least squares line. This is again achieved by computing the principal components of each column and then projecting out the component associated with the smaller eigenvalue. The resulting points are then projected back to the original space by multiplying them by the row plane vectors. To complete the transformation back into the initial coordinates the mean position of each optode loci row, which was subtracted initially, is re-added to that row.

Correction of errors in marker position

Errors in localizing the 10–20 reference points on participants' skulls result in an exaggerated distance between the optode loci and the surface of the skull. Thus, an error in one position could potentially cause a bias in the position of all optodes. Moreover, the distance from the skull reflects a possible discrepancy between the curvature of the reconstructed holder geometry and the skull shape, which could cause a change in the angle of the normal to the surface. However, if the markers were shifted to their correct positions, then the average distance would be greatly reduced and the estimation accuracy of the holder curvature would be increased. Therefore, allowing the recorded reference points to vary in position within the bounds of

the measurement error until this distance is minimized would correct for the initial error.

This can be formalized as a straightforward optimization problem in the following manner. Let $Af : \Re^{3 \times k \times 2} \to \Re^{3 \times 3}$ be the function that matches pairs of ordered sets of k 3D points with a unique affine transformation matrix B, and let $D_{head} : \Re^{3 \times n} \to \Re$ be the function that matches each set of n 3D points with the mean distance to the skull surface. Therefore, to correct such errors the expression $\underset{v}{\arg\min}\, D_{\text{head}}(Af(V + [\quad 0 \quad \cdots \quad v \quad \cdots \quad 0], M)(Opt))$ needs to be solved for each reference point v_i sequentially, where Opt denotes the optode loci set (matrix), V the real-world markers and M the corresponding 10–20 markers in MNI space. To keep the solution ecologically valid, two additional constraints need to be placed: change in each coordinate for the reference point must be bound by the degree of measurement error and change in orientation of the mid-plane (to which optode rows are parallel) after the correction must not exceed some reasonable limit. That is, for each measured reference point $|v_{ix} - v_x|, |v_{iy} - v_y|, |v_{iz} - v_z| < \varepsilon$, and $angle\,(Af(V, M)(Opt), Af\,(V + [0 \cdots v \cdots 0], M)(Opt)) < \theta$, where the $angle$ matches each set of optode loci with a mid-plane (see preceding section).

By carrying out repeated measurements of single markers, we acquired independent measurements to establish the error bounds of individual marker measurements and found that error was contained within a 5-mm sphere. Accordingly, when applying the optimization to our data we limited the search volume to this range. As a bound on θ we made a conservative choice of 1°.

We chose to utilize the pattern search algorithm (Lewis and Torczon, 1999) to solve the abovementioned problem. This is a gradient free global optimization algorithm for bound non-linear optimization problems that solves problems iteratively through grid refinements until the objectives are met.

Projection to the brain and reconstruction of optode holder geometry

After correction of measurement errors, the optode loci can be used to reconstruct the holder surface. This can be done by fitting the optode contacts with a thin plate spline (Bookstein, 1989; Duchon, 1977). A thin plate spline (TPS) is the smooth surface f that passes through a given set of control points (i.e., the optode contacts in our case) while minimizing the bending energy: $BE = \iint \left[\left(\frac{\partial^2 f}{\partial x^2}\right)^2 + 2\left(\frac{\partial^2 f}{\partial x \partial y}\right)^2 + \left(\frac{\partial^2 f}{\partial y^2}\right)^2 \right] dxdy$. It is this latter property that makes this model appropriate for the current setting.

Let $x \in \Re^2$ be a query point and $\{c_i\} \in \Re^2$ a set of control points. The thin plate spline describing the smooth surface connecting these points is $TPS(x) = \sum_i w_i \Phi(r_i) + \sum_{j=1}^{2} b_j x_j + b_0$, where $r_i = \|x - c_i\|$ and $\Phi\,(r) = r^2 \ln\,(r)$ (apart from $r = 0$ where $\Phi = 0$), w_i are the coefficients of the higher order terms and b_i the linear coefficients. As a TPS is a 2D model it is necessary to rotate the data appropriately before fitting control points with the surface (e.g., by finding the rotation maximizing the z coordinate of the optode contacts). After applying this rotation the model can be fit by solving the linear system $X \begin{bmatrix} w \\ b \end{bmatrix} = Opt(z)$ (where $Opt(z)$ denotes the z coordinates of the optode contacts) and $X = \begin{bmatrix} \Phi & A \\ A^t & 0 \end{bmatrix}$ (where $\phi_{ij} = d(Opt(xy)_i, Opt(xy)_j)^2 \ln(d(Opt(xy)_i, Opt(xy)_j))$, $d(\cdot, \cdot)$ is the Euclidean distance function and the rows of the matrix A are given by $A_i = [Opt(x)_i\, Opt(y)_i\, 1])$.

Once the holder model has been fitted to the optode loci, the model can be used to correct residual measurement errors in optode positions and strictly enforce the ground truth by embedding the optode contacts within the estimated skull surface. This is achieved by isometrically embedding the geodesics connecting the optode loci within the skull surface. To do so, the geodesics must first be numerically approximated. We have found that an effective way of

achieving this is by using a cubic spline (see Appendix) connecting the control points as an initial guess and then embedding it within the holder model by projection along the normal at each point. The normal to a spline curve is given by $n = \gamma''(t) - \langle \gamma''(t), \gamma'(t) \rangle / \|\gamma'(t)\|^2$ where $\gamma'(t)$ is the tangent to the spline.

Once the geodesics are approximated, the midpoint of the model is forced to make contact with the skull surface by projecting along the normal to the holder model surface (see details below). The intersection of the middle optode plane and the skull surface can then be found. The resulting set of points is fitted with a smoothing spline (Reinsch, 1967; see Appendix), which represents the cross section as a smooth dense curve. Next, the distance between the control points along the geodesics is computed numerically, and the corresponding points matching the optode-to-optode distances on the skull contour are found (again with the arc-length formula above). This is first done for the midline (column) geodesic of the holder model and then for each optode row in turn. The end result is a minimally distorted embedding of the optode loci, which preserves distances and angles to the extent possible.

Finally, the rectified optode positions can be refit with a holder model and the computed normal can be used to project the optode contacts onto the cortical surface. To compute the normal of the surface it is convenient to express the surface implicitly as $F(x, y, z) = z - TPS(x, y)$. Under this representation, the surface is given by points satisfying $F(x, y, z = 0)$. Thus, the normal is given by the gradient of the function (as it is orthogonal to the level set): i.e., $\nabla F(x, y, z) = \left[-\dfrac{\partial TPS}{\partial x}(x, y) \quad -\dfrac{\partial TPS}{\partial y}(x, y) \quad 1 \right]^t$ where $\dfrac{\partial TPS}{\partial x} = \sum_i w_i(x - c_{xi})(1 + 2 \log(r))$. Consequently, the normal at an optode contact Opt_i can be computed explicitly and used to project the contact point to the cortical surface. If N_i denotes the normal to the ith contact point and D_{ctx} the distance function to the
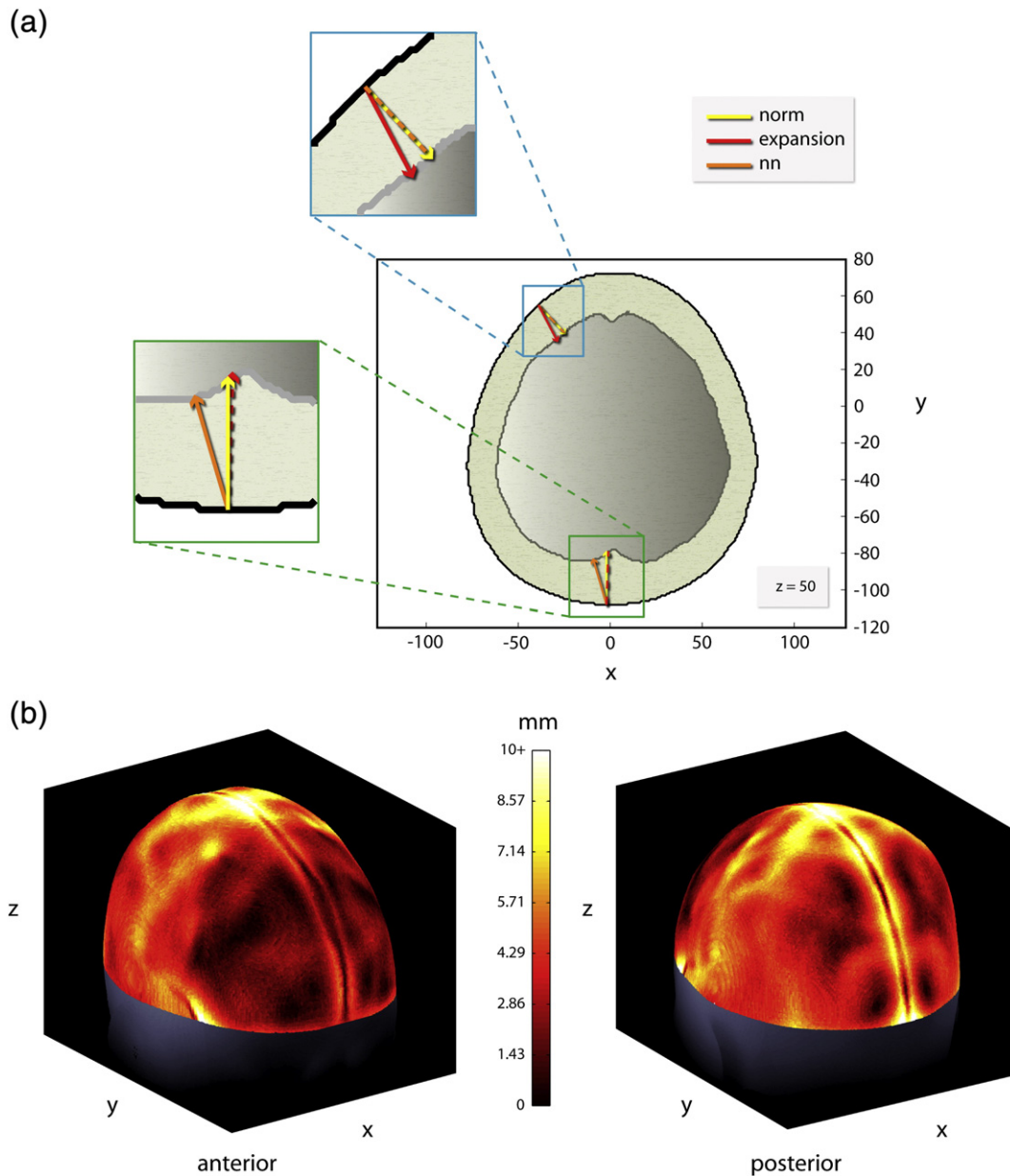
Fig. 1. The importance of exact cortical projection methods. (a) A horizontal slice ($z = 50$) of the contours of the brain and skull taken from the MNI brain. Two points on the skull were selected and projected to the cortical surface via three methods: finding the nearest neighbor (NN), cortical expansion, and projecting along the normal to the skull. Even in the simplified 2D scenario, the discrepancy between the exact method and the approximation can be as much as 5 mm. (b) A comparison of the balloon inflation method (Okamoto et al., 2004) to projection along the normal to the skull. Each point on the skull surface of the MNI brain was projected to the cortical surface using the two methods and the Euclidean distance between each pair of points corresponding to a given point on the skull was measured. On average, the discrepancy was about 4 mm (3.83 ± 1.9 mm).

set of cortical surface points, then the optode radiation is found by solving $\arg\min\limits_{a} D_{ctx}(Opt_i + aN_i)$.

Establishing channel positions

Once the optodes have been projected to the cortical surface, they can be transformed to MNI space and the channel loci can be established. A channel is defined as the midpoint between two optode (i.e., source detector pair) radiations. Thus, to localize a channel position on the cortical surface, it is necessary to first intersect the equidistant plane to the radiations with the cortical surface and then locate the point that minimizes the distance to the radiations. Let Ctx denote the cortical surface in MNI space and Opt_i and Opt_j the two radiations. A point v on the equidistant plane satisfies $\langle v, Opt_i - Opt_j = 0\rangle$. Thus, if $n_{ij} = \frac{1}{||Opt_i - Opt_j||}(Opt_i - Opt_j)$, the distance of a point $x \in Ctx$ to this plane is $\langle x - m_{ij}, n_{ij}\rangle$, where $m_{ij} = \frac{1}{2}(Opt_i + Opt_j)$. Let Ctx_{ij} be the set of points in Ctx that are at most a voxel away from the equidistant plane. A channel is given by the member of this set that minimizes the distance to both radiations, $Chnl_{ij} = \min\limits_{x \in Ctx_{ij}}(d(x, Opt_i) + d(x, Opt_j))$, where $d(\cdot, \cdot)$ denotes the Euclidean distance function.

Estimation of the localization error bounds due to anatomical differences

Okamoto et al. (2004) suggest the following method to assess the error bounds of localization due to anatomical differences between a subject's actual brain, and the target template (e.g., the MNI brain): rather than projecting the measured optode positions to MNI space directly through utilizing the measured anatomical landmarks, the optode loci are computed on a database of 17 brains, each of which is used as the target template. This is followed by projecting the resulting loci to the MNI brain using an affine transformation based on the 10/20 markers (see Forward and backward transformation into MNI space). This allows one to compute the spatial deviation in position after transformation to MNI space for the resulting 17 projections. The spatial deviation is given by the standard deviation of xyz coordinates—the square root of the pooled variance.

The same method can be applied to estimate the localization error bounds due to anatomical differences for our projection algorithm. To do so, our method is applied to the initial measurements using each of the 17 reference brains, in place of the MNI brain, as a target template. Next, each resulting set of loci (17, one for each brain) is transformed to MNI space.

Estimating the effect of denoising on localization accuracy

To assess the effect of denoising on the accuracy of cortical localization, analysis is carried out on the distribution of optode radiations at the group level. To this end, the method described above is applied to data with and without denoising (i.e., in the latter scenario, data were simply fit with a holder model as is). In our experiment, the optode holder was positioned on participants' heads by aligning the middle optode shaft with the midline of the back of the skull. In the ideal scenario, if one were to obtain perfect measurements, one would expect no variance in optode position across subjects for the middle optode shaft. If so, the further away optode shafts are, the more divergence one would find resulting from variation in head size. Therefore, the average distance of optode radiations to the respective group centroids (i.e., the average position for each optode across subjects) is expected to increase as a function of distance from the mid-optode centroid. Accordingly, in order to compare the average distance to optode centroids between the two projection methods, this effect needs to be factored out.

To model the effect of distance from middle on position divergence, the points are fit with a quadratic linear model. Therefore,

to estimate the fraction of cluster divergence resulting solely from noise, the fraction of variance explained by distance (i.e., the quadratic trend) is regressed out of the data if the fit is significant. The remaining difference between groups results purely from the difference in the denoising procedures.

Results

Okamoto and Dan (2005) suggest that the exact method of projecting optode skull positions to the cortical surface is by computing the normal to the tangent plane at the point of contact. However, for practical reasons they suggest using approximate methods. Therefore, we set out to determine to what extent employing approximate methods results in consistent deviation from projection along the normal. We compared three approximate methods of projection to projection along the normal: *nearest neighbor (NN)*, *cortical expansion (CE)*, and *balloon inflation* (Okamoto et al., 2004, 2005; Singh et al., 2005; see Approximate projection methods).

In Fig. 1a, a horizontal section ($z = 50$) of the skull and brain surface of the MNI template are shown. Even in the 2D case the discrepancy between normal projection and the NN and CE methods can exceed 5 mm. The results of the comparison between the normal projection and the balloon inflation method are shown in Fig. 1b. This method results in considerable bias: on average, 3.83 ± 1.9 mm.

We corrected the raw optode position measurements by enforcing geometric constraints, reflecting the optode holder structure on the measurements. Optode rows and columns were made parallel and optode positions were evenly spaced (see Correction of errors in optode locations). Fig. 2 shows the results of this procedure applied to the measurements taken from a representative participant. As can be seen, after application of these constraints, the measurements reflect the actual physical state with greater accuracy.

Next, we corrected error in the marker positions by finding the displacement that would minimize the optode-to-skull distance in MNI coordinates. This was achieved by a constrained optimization procedure (see Correction of errors in marker position), which maintained the orientation of the optode positions, while searching in a volume determined by an independent assessment of the error measurement. In our data, without correction, after projection into MNI space the average distance of the optode loci to the cortical surface was 6.1 ± 4.25 mm. As can be seen in Fig. 3a, the above optimization reduced the optode-to-skull distance as well as standard deviation from 6.1 ± 4.25 mm to 2.55 ± 2.27 mm, respectively. As illustrated in Fig. 3b, the convergence properties of this method are
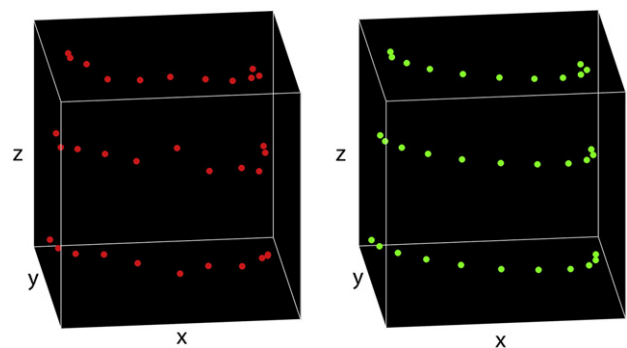
Fig. 2. Correcting errors in optode position via geometrical constraints. In NIRS experiments, optodes are secured to participants' scalps by an optode holder. The well-defined geometry of the holder can be used to derive constraints that allow one to reduce measurement error for individual optode positions. In this case, the original measurements (*red*) were forced to lie on parallel planes (rows and columns) by regression to the least squared planes (i.e., the principle components) and were evenly spaced (row-wise) on cubic spline curve fits. The result is shown in green.
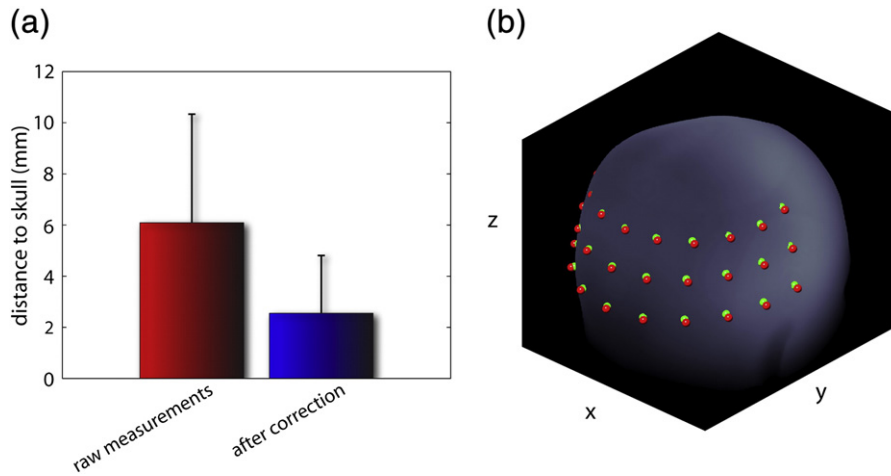
Fig. 3. Correction of measurements of anatomical landmarks. Measurement errors in localizing the markers on the skull surface can result in optode positions that are "free-floating." After being affine transformed to MNI space optodes can be removed from the skull surface by as much as 1 cm (6.1 ± 4.25 mm). Measurement errors can be reduced by non-linear bound optimization in which marker positions are varied within the bounds of the observed measurement error (~5 mm), such that the new affine transformation to MNI space yields the minimal average distance of the optode positions to the skull. This is done under the constraint that the resulting points will maintain an orientation that is removed by at most one degree from the orientation of the original transformed points. (a) After optimization, the average distance to the skull is reduced as is the associated standard deviation (6.1 ± 4.25 mm compared with 2.55 ± 2.27 mm). (b) The average group optode positions are shown before (*red*) and after (*green*) correction (both following geometric correction).
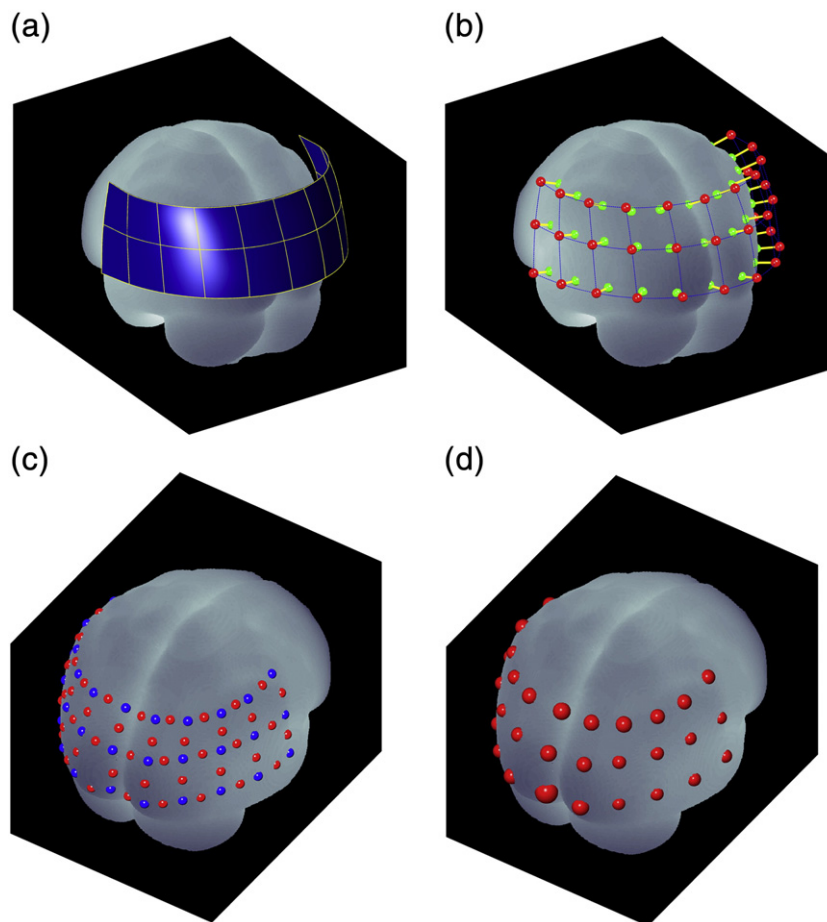
Fig. 4. Registration of corrected measurements to the cortical surface. The process is illustrated with data from a representative participant. (a) The optode holder model. After correction for measurement errors, the optode positions are fitted with a smooth surface: a thin plate spline (TPS). The numeric approximations of the geodesics are overlaid on the model surface in yellow. These are used to numerically approximate an isometric embedding to the ideal skull template. (b) The advantage of explicitly modeling the optode holder as a parametric surface (contours in blue) is the ability to compute the surface normals exactly (*yellow*), thus enabling one to project the optode/skull contact points (red) to the cortical surface (*green*). (c) After projecting the optodes to the brain (*blue*), the channel positions can be computed (*red*). (d) To assess the uncertainty in position resulting from individual anatomical variance, the same procedure was carried out on the reference set of 17 brains (Okamoto et al., 2004, 2005; Singh et al., 2005). The results were then transformed to MNI space and the associated standard deviation computed. The error on average was 4.32 ± 0.62 mm, while for the method of Okamoto and Singh et al. (Okamoto et al., 2004, 2005; Singh et al., 2005), the average error was 6.12 ± 1.24 mm – $p < 1 \times 10^{-7}$ on a two-sample t-test ($df = 32$). The same was true for all 12 participants (4.36 ± 0.82 vs. 6.24 ± 1.39 mm, $p < 1 \times 10^{-91}$ on a two-sample t-test ($df = 395$)).

very satisfactory: in red, the average optode positions for all participants (after correction for optode position error, $N=12$) are displayed next to the MNI skull surface and, in green, after application of the above algorithm.

Next, residual errors in optode positions were corrected by isometric embedding (see Projection to the brain and reconstruction of optode holder geometry). As a result, optode loci were strictly embedded in the real-world coordinate estimate of each participant's skull surface (computed via the backward MNI transform; see Forward and backward transformation into MNI space). Finally, the optodes were fitted with an explicit surface modeling the holder, which in turn allowed us to project optode loci to the cortical surface, and subsequently to MNI space via the forward transform (see Forward and backward transformation into MNI space). The results of the above procedure applied to the same representative participant of Fig. 3 are shown in Fig. 4a and b. We then determined channel positions (see Establishing channel positions) for each subject. Fig. 4c shows the channel positions (blue) alongside the optode loci for that same subject.

To assess the error bounds of localization due to anatomical differences, we followed the method suggested in Okamoto et al. (2004; see Estimation of the localization error bounds due to anatomical differences), which utilized their reference set of 17 brains. For our representative participant, the error on average was 4.32 ± 0.62 mm while for the method of Okamoto et al. (2004, 2005) the average error was 6.12 ± 1.24 mm; $p < 1 \times 10^{-7}$ on a two-sample t-test ($df=32$). The error bounds for our representative subject are shown in Fig. 4d, represented by the diameter of the optode markers.

The same was true for all 12 participants (4.36 ± 0.82 vs. 6.24 ± 1.39 mm – $p < 1 \times 10^{-91}$ on a two-sample t-test ($df=395$)). Fig. 5 shows a comparison of the results of our method and the method described in Okamoto et al. (2004, 2005) for our representative participant, as well as one other participant in our sample.

To assess the effect of denoising on the accuracy of cortical localization, we carried out analyses on the distribution of optode radiations at the group level. To this end, we applied the method described in Estimating the effect of denoising on localization accuracy to our data, with and without denoising (i.e., in the latter scenario data was simply fit with a holder model as is). Prior to further analysis it was necessary to discard the data of three subjects due to faulty initial placement of the optode holder (see Supplementary Fig. 1).

In Fig. 6b, the average distances to each optode centroid (average optode position across subjects) after computing optode positions with (green) and without denoising (red) are shown. As can be seen, after denoising, points exhibit a clear effect of distance to the mid-optode. The effect of distance from the middle on position divergence was modeled with a quadratic linear model (Estimating the effect of denoising on localization accuracy). Indeed, a significant fit was found for the denoised data ($F=64.36$, $df=(2,30)$, $p<10^{-8}$, shown in black in Fig. 6b). However, for data that weren't denoised, the underlying structure was masked by noise and no such trend was found ($F=2.46$, $df=(2,30)$, $p>0.1$). Therefore, to estimate the fraction of cluster divergence resulting solely from noise, the fraction of variance explained by distance (i.e., the quadratic trend) was regressed out of the denoised data (Estimating the effect of denoising on localization accuracy; Fig. 6c). The remaining difference between groups results purely from the denoising procedures. The difference is on average 3.45 mm ($p<10^{-25}$ on a one-sided t-test, $df=32$). This means that, on average, the group optode radiation clusters shrunk in diameter by 7 mm. The distribution of group optode radiations before (green) and after (red) denoising are shown in Fig. 6d–e. As can be seen, denoising tightens group position clusters significantly.

The distribution for optode positions registered by the method of Okamoto and Singh et al. (Okamoto et al., 2004, 2005; Singh et al.,
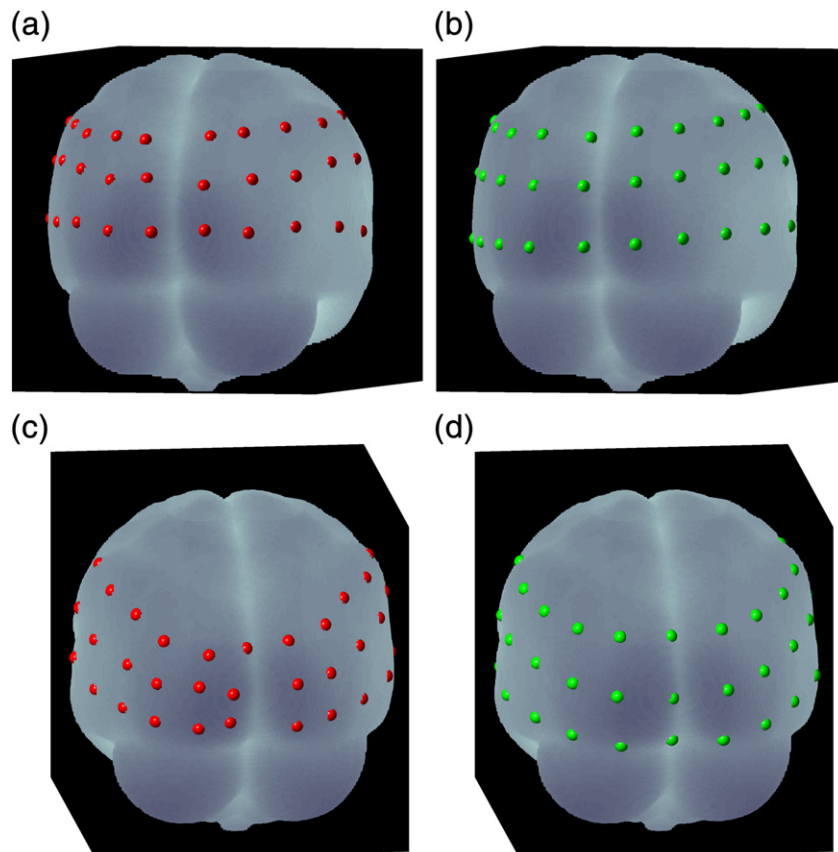

Fig. 5. Comparison to the probabilistic method (Singh et al., 2005). (a) The registered optodes of a participant using the algorithm described by Okamoto and Singh et al. (Okamoto et al., 2004, 2005; Singh et al., 2005). (b) The registered optodes applying the procedure described in this manuscript. (c–d) The same for an additional participant.
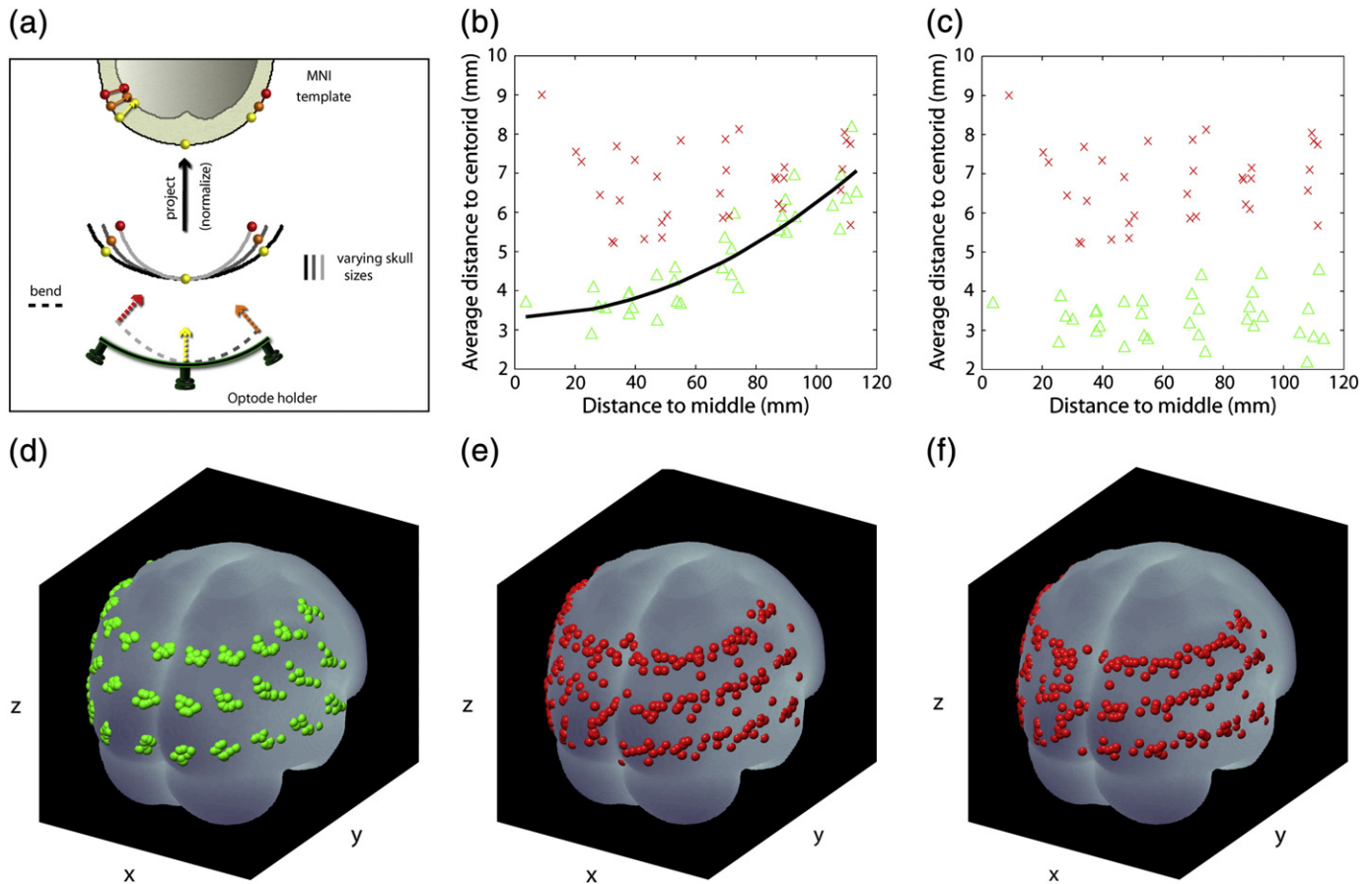
Fig. 6. The effect of denoising on registration accuracy. (a) A schematic illustration depicting the source of the distance dependency. If a curved optode holder is fixed to the skull of people with varying head sizes by positioning its center according to some fixed anatomical marker (e.g., inion) the variance across subjects will be minimal in the center position and increase as a function of distance from the center (b) The distribution of average distance of optode radiations to the group centroid as a function of distance from the mid-optode centroid. Each point represents the average distance across subjects for a given optode to the average position of that optode. In *red*, points derived from projection after fitting optode positions with a smooth plate spline model without denoising. In *green*, points derived following the complete procedure described above. As can be seen, after denoising, points exhibit a clear effect of distance from the mid-optode. In *black*, the fit of a quadratic linear model ($F = 64.36$, $df = (2,30)$, $p < 10^{-8}$). The red points do not exhibit such a trend ($F = 2.46$, $= (2,30)$, $p > 0.1$); the underlying structure is masked by noise. (c) The same points in (a) after the fraction of variance explained by distance (i.e., the quadratic trend) is regressed out. The remaining difference between groups results purely from the denoising procedures. The difference is on average 3.45 mm ($p < 10^{-25}$ on a one-sided *t*-test, $df = 32$). This means that, on average, the diameter of the group optode radiation clusters grows tighter by 7 mm. (d–e) The distribution of group optode projections before (*red*) and after (*green*) denoising. As can be seen, denoising tightens group position clusters significantly. (f) The distribution of optode positions registered by the method of Okamoto and Singh et al. (Okamoto et al., 2004, 2005; Singh et al., 2005). The same analysis as in (b) shows that with this method distance dependency is again masked ($F = 0.95$, $df = (2,30)$, $p > 0.39$ for the fit to a quadratic model). A comparison after distance dependency is regressed out yielded an average difference of 2.56 mm ($p < 10^{-13}$, $df = 32$). Thus, on average our method yielded a tightening of the diameter of group optode position clusters by 0.5 cm.

2005) is shown in Fig. 6f. We applied the same analysis (Estimating the effect of denoising on localization accuracy) to these data, and again found that distance dependency is masked ($F = 0.95$, $df = (2,30)$, $p > 0.39$ for the fit to a quadratic model). A comparison, after distance dependency was regressed out from the denoised data, yielded an average difference of 2.56 mm ($p < 10^{-13}$, $df = 32$). Thus, on average our method yielded a tightening of the diameter of group optode position clusters equal to 0.5 cm.

Discussion

Here we describe a method of localizing NIRS measurements in MNI (or any other standard template) space without MRI, as implemented in our publicly available toolbox, the NIRS Analysis Package (NAP: http://lsec.neuropraxia.webfactional.com/Software_and_Instrumentation.html). This method comprises the following steps:

- Correct optode positions to correspond to holder geometry.
- Correct 10–20 system marker positions by finding the displacement that results in an affine transformation B to MNI space that minimizes the optode to cortical surface distance.

- Fit optode loci with a thin plate spline modeling the optode holder.
- Correct residual error in optode positions by isometric embedding of the holder model in the estimated skull surface (i.e., $B^{-1}(H_{MNI})$)
- Refit the embedded optode loci with a thin plate spline model.
- Project optodes along the normal to the holder model surface to the estimate of the cortical surface.
- Transform optode projections to MNI space and compute channel positions.

We show that this method is consistent: as has been previously reported for the method of Okamoto and Singh et al. (Okamoto et al., 2004, 2005; Singh et al., 2005), the error bounds resulting from individual anatomical differences are within 1 cm. However, due to the explicit modeling of the optode holder, it is now also possible to avoid inherent inaccuracies in the localization of optode radiations and moreover, to denoise the original measures by enforcing constraints derived from its geometry.

Due to reduction in projection inaccuracies (Fig. 1), reduced error resulting from anatomical variation (Fig. 4) and increased accuracy afforded by denoising procedures (Fig. 6), our method achieved increases in accuracy of at least 6 mm (on average) compared to the

commonly used method of Okamoto and Singh et al. (Okamoto et al., 2004, 2005; Singh et al., 2005). In worst-case scenarios, our method increases accuracy by over 1 cm. The outcome of this procedure is a set of points that best represents the ground truth at the time of measurement.

Supplementary materials related to this article can be found online at doi:10.1016/j.neuroimage.2011.03.068.

Acknowledgments

Appendix: Natural and smoothing splines

A natural spline is function constructed of piecewise third-order polynomials that pass through a set of control points, $\{Y_i\} \in \Re^n, i = 0 \ldots k$. We will describe the 1D case for simplicity's sake as multidimensional splines are simply constructed from fitting splines to each coordinate.

The pieces' splines are parameterized by $t \in [0\ 1]$, and follow the form: $Y_i = a_i + b_i t + c_i t^2 + d_i t^3$. The derivatives and second derivatives of the pieces are forced to coincide in the control.

The second derivative of each polynomial is set to zero at the endpoints, since this provides a boundary condition that completes the system of equations. This produces a so-called "natural" cubic spline and leads to a simple tridiagonal system, which can be solved to give the coefficients of the polynomials, i.e.,

$$
\begin{bmatrix}
2 & 1 & & & & & & 0 \\
1 & 4 & 1 & & & & & \\
& 1 & 4 & 1 & & & & \\
& & 1 & 4 & 1 & & & \\
& & & & \ddots & & & \\
& \ddots & & & & 1 & 4 & 1 \\
0 & & & & & & 1 & 2
\end{bmatrix}
\begin{bmatrix}
b_0 \\ b_1 \\ b_2 \\ b_3 \\ \vdots \\ b_{k-1} \\ b_k
\end{bmatrix}
=
\begin{bmatrix}
3(y_1 - y_0) \\
3(y_2 - y_0) \\
3(y_3 - y_1) \\
3(y_4 - y_2) \\
\vdots \\
3(y_k - y_{k-2}) \\
3(y_k - y_{k-1})
\end{bmatrix}.
$$

A smoothing spline results from adding a smoothing term to the polynomial pieces. In this scenario the spline no longer strictly passes through the control points but rather minimizes the expression: $p \sum_i (y_i - S_i(0))^2 + (p-1) \int \left(\frac{d^2 s}{dx^2} \right)^2 dx$. Hence, the parameter p controls the degree of smoothing, ranging from 1 in which there is no smoothing to 0, in which there is maximal smoothing.

References

Bookstein, F., 1989. Principal warps: thin-plate splines and the decomposition of deformations. IEEE Trans. Pattern Anal. Mach. Intell. 11, 567–585.

Cope, M., Delpy, D.T., Reynolds, E.O., Wray, S., Wyatt, J., van der Zee, P., 1988. Methods of quantitating cerebral near infrared spectroscopy data. Adv. Exp. Med. Biol. 222, 183–189.

Duchon, J., 1977. Splines minimizing rotation-invariant semi-norms in Sobolev spaces. Constructive theory of functions of several variables, 85–100.

Fukui, Y., Ajichi, Y., Okada, E., 2003. Monte Carlo prediction of near-infrared light propagation in realistic adult and neonatal head models. Appl. Opt. 42, 2881–2887.

Huppert, T.J., Diamond, S.G., Franceschini, M.A., Boas, D.A., 2009. HomER: a review of time-series analysis methods for near-infrared spectroscopy of the brain. Appl. Opt. 48, D280–D298.

Jasper, H., 1958. The 10–20 electrode system of the International Federation. Electroencephalogr. Clin. Neurophysiol. 10, 371–375.

Jobsis, F.F., 1977. Non-invasive, infra-red monitoring of cerebral O2 sufficiency, blood-volume, HbO2-Hb shifts and bloodflow. Acta Neurol. Scand. Suppl. 64, 452–453.

Lewis, R., Torczon, V., 1999. Pattern search algorithms for bound constrained minimization. SIAM J. Optimization 9, 1082–1099.

Okada, E., Delpy, D., 2003a. Near-infrared light propagation in an adult head model. I. Modeling of low-level scattering in the cerebrospinal fluid layer. Appl. Opt. 42, 2906–2914.

Okada, E., Delpy, D., 2003b. Near-infrared light propagation in an adult head model. II. Effect of superficial tissue thickness on the sensitivity of the near-infrared spectroscopy signal. Appl. Opt. 42, 2915–2922.

Okamoto, M., Dan, H., Sakamoto, K., Takeo, K., Shimizu, K., Kohno, S., Oda, I., Isobe, S., Suzuki, T., Kohyama, K., Dan, I., 2004. Three-dimensional probabilistic anatomical cranio-cerebral correlation via the international 10–20 system oriented for transcranial functional brain mapping. Neuroimage 21, 99–111.

Okamoto, M., Dan, I., 2005. Automated cortical projection of head-surface locations for transcranial functional brain mapping. Neuroimage 26, 18–28.

Reinsch, C., 1967. Smoothing by spline functions. Numerische Mathematik 10, 177–183.

Singh, A.K., Okamoto, M., Dan, H., Jurcak, V., Dan, I., 2005. Spatial registration of multichannel multi-subject fNIRS data to MNI space without MRI. Neuroimage 27, 842–851.